

Rayleigh-Taylor instability in elastic-plastic solid slabs bounded by a rigid wallS. A. Piriz,^{1,2} A. R. Piriz¹, N. A. Tahir,³ S. Richter,² and M. Bestehorn²¹*Instituto de Investigaciones Energéticas (INEI), E.T.S.I.I., and CYTEMA, Universidad de Castilla-La Mancha, 13071 Ciudad Real, Spain*²*Department of Statistical Physics and Nonlinear Dynamics, Brandenburg University of Technology, 03044 Cottbus-Senftenberg, Germany*³*GSI Helmholtzzentrum für Schwerionenforschung Darmstadt, Planckstrasse 1, 64291 Darmstadt, Germany*

(Received 22 August 2020; revised 17 January 2021; accepted 22 January 2021; published 10 February 2021)

The linear evolution of the incompressible Rayleigh-Taylor instability for the interface between an elastic-plastic slab medium and a lighter semi-infinite ideal fluid beneath the slab is developed for the case in which slab is attached to a rigid wall at the top surface. The theory yields the maps for the stability in the space determined by the initial perturbation amplitude and wavelength, as well as for the transition boundary from the elastic to the plastic regimes for arbitrary thicknesses of the slab and density contrasts between the media. In particular, an approximate but very accurate scaling law is found for the minimum initial perturbation amplitude required for instability and for the corresponding perturbation wavelength at which it occurs. These results allow for an interpretation of the recent experiments by Maimouni *et al.* [*Phys. Rev. Lett.* **116**, 154502 (2016)].

DOI: [10.1103/PhysRevE.103.023105](https://doi.org/10.1103/PhysRevE.103.023105)**I. INTRODUCTION**

The Rayleigh-Taylor instability (RTI) has been extensively studied when the involved media are fluids, and the underlying physical mechanism is rather well understood in many different scenarios [1–7]. However, RTI taking place in solid media is much less understood although it has implications in many different fields such as geophysics [8], astrophysics [9–12], planetary science [13–22], and material science [23–26]. It also plays a role in many problems of high energy density (HED) [27–36]. In fact, RTI has important implications in laboratory experiments in which matter is taken to extreme states by means of the acceleration of shells and plates driven by very high pressures.

At such extreme conditions a solid behaves as a deformable medium, first as an elastic medium and then as a plastic one. Of course, depending on the driving conditions it may later become successively a fluid, an ideal gas, and a plasma. But in the solid phase, the nonlinear character of the constitutive material properties clearly distinguishes RTI in solid media from its fluid counterparts, making its analysis and the construction of a compelling theory much more involved.

With the focus on the instability of metal plates accelerated by high explosives, Miles performed in 1966 the first theoretical analysis of the problem of RTI in solids by considering a simple physical model known as the one-degree-of-freedom model [37]. Such a model would be adopted by other researchers in the following years yielding different predictions that, although of showing a qualitative agreement with some of the features of the RTI in solids, they turned out quantitatively inaccurate when compared with the numerical simulation results and experiments. In particular, such models failed to account for the transition from the elastic to the plastic regime of the instability [32,33,38].

On the other hand, experiments on RTI in solids were performed by Barnes *et al.* [34]. These and subsequent analytical, experimental, and numerical simulation works showed that the stability conditions of the linear RTI in elastic-plastic solid materials is not determined only by the perturbation wavelength as it occurs in fluids (for given gravity acceleration and slab thickness), but also by the amplitude of the initial perturbation [35,39,40].

A physical model based on the second law of Newton that produced approximate but very accurate results, was developed to consider a semi-infinite perfectly elastic medium [19,41], and it was also applied to a semi-infinite elastic-plastic solid medium for the case of Atwood number $A_T = 1$ ($A_T = (\rho_2 - \rho_1)/(\rho_2 + \rho_1)$, where ρ_2 and ρ_1 are the densities of the heavier and lighter media, respectively) [42,43]. In the latter case, it was shown that the elastic and the plastic regimes could be treated as successive phases, and thus, it was established that a stability criterion pointed out that, in general, the transition to the plastic regime is a necessary but not a sufficient condition for instability. In later works, the application of this approximate irrotational model was extended for considering $A_T < 1$, and interfaces with viscous fluids and with regions filled by magnetic fields [44,45].

The exact linear theory for the RTI in accelerated elastic solid slabs (with a free surface) of arbitrary thickness was developed by Plohr and Sharp for the particular case of $A_T = 1$ [46], and it was recently extended to arbitrary Atwood numbers [47]. The latter work was based on the normal modes method and yields analytical expressions for the dispersion relation from which the instability growth rate in slabs of arbitrary thickness is obtained. The work shows that the vorticity generation cannot be neglected when relatively thin slabs are considered. In addition, it also includes the results by Terrones for semi-infinite media and arbitrary Atwood number [48].

More recently, the linear RTI in a perfectly elastic (Hookean) slabs of thickness h and shear modulus G attached to a rigid wall and subject to a gravity g (equal to the Earth gravity) has been experimentally and theoretically studied by Mora *et al.* [49], including surface tension effects and for $A_T = 1$. They have found an expression for the dimensionless slab thickness $\alpha = \rho_2 g h / G$ as a function of the dimensionless cut-off wave number $k_c h$ (for which the instability growth rate is zero. $k = 2\pi/\lambda$ where λ is the perturbation wavelength) and, although they do not present an explicit form for the dispersion relation, the instability growth rate is shown in a graphical representation. In addition, they have pointed out the existence of an instability threshold for $\alpha \approx 6.223$, below which the system is stable for any perturbation wave number. The same problem was somewhat later studied theoretically in Ref. [50] for arbitrary Atwood numbers, but the general expression for the dispersion relation was still missing.

Very recently, a different category of experiments using soft matter has been reported, in which the material exhibits its elastic-plastic properties under conditions of Earth gravity or some few times the Earth gravity [51–53]. These experiments are also necessarily performed in contact with a rigid wall, in contrast to the free surface situation present in the HED experiments. However, this set of experiments are complementary of those performed in the framework of HED physics, since the underlying physics is analog. Therefore, they represent an excellent work scenario that can contribute to shed light on the basic physics of the RTI in solids, and can serve for testing theories and numerical simulation calculations. In addition, the elastic-plastic constitutive properties of these materials can be well characterized and the parameters can be controlled more easily, which allows for the achievements of a higher experimental precision. Moreover, since extreme conditions are not required, big and expensive facilities and set ups (high explosives, high intensity lasers or ion beams) are not needed, making them much more accessible to small laboratories with relatively modest technical and economical resources. In summary, such experiments can aid to the construction of a wide experimental database with potential benefits for the research on RTI in solids under HED physics conditions.

Therefore, it is of great interest to extend the existing theories for RTI in accelerated solids to the situation in which the solid is in contact with a rigid wall. Such small scale experiments may also provide a validation for the theoretical approach currently used in the description of large scale HED experiments.

In this work we extend and generalize previous results with the aim of providing a theoretical framework for the interpretation of some of the existing RTI experiments involving elastic-plastic media performed in the presence of a rigid wall. For this purpose, we will determine the corresponding stability region such as it is defined by the wavelength and the initial amplitude of the perturbations.

II. LINEAR ANALYSIS OF THE INSTABILITY

We start with the consideration of an horizontal elastic-plastic solid slab of density ρ_2 and thickness h that occupies the region $-h \leq y \leq 0$, is subject to a uniform gravity acceleration $\mathbf{g} = g\mathbf{e}_y = -\nabla\varphi$ (\mathbf{e}_y is the unitary vector in the vertical

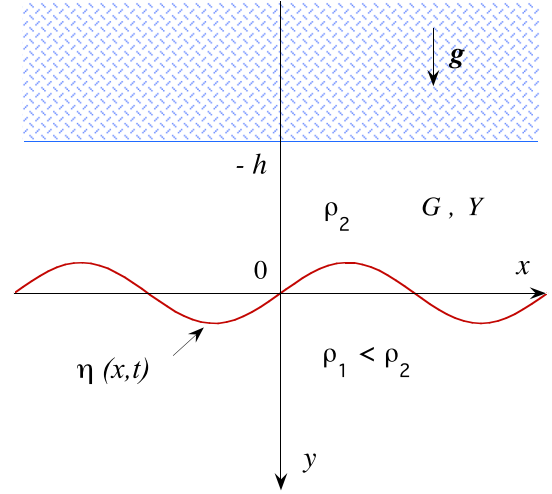


FIG. 1. Schematic of an elastic-plastic slab bounded by a rigid wall on the top ($y = -h$), and by an unstable interface with a semi-infinite ideal fluid on the bottom ($y = 0$).

direction and φ is the gravitational potential), and is in contact with a rigid wall at $y = -h$, while an ideal fluid of density $\rho_1 < \rho_2$ occupies the semi-infinite space $y > 0$ beneath the slab (Fig. 1). The elastic-plastic constitutive properties of the slab are characterized by the shear modulus G and the yield strength Y , and the media are assumed incompressible and immiscible [42,54]. The two-dimensional (2D) situation with an initially flat interface, is schematically represented in Fig. 1 after a sinusoidal disturbance $\eta(x, t)$ has been applied.

The governing equations for the mass and momentum conservation for incompressible continuous media read, respectively,

$$\frac{\partial v_{ni}}{\partial x_i} = 0, \quad (1)$$

$$\rho_n \frac{dv_{ni}}{dt} = -\frac{\partial p_n}{\partial x_i} + \rho_n g_i + \frac{\partial \sigma_{ik}^{(n)}}{\partial x_k}, \quad (2)$$

where $n = 1, 2$, refer to the bottom and top media, respectively, and index notation for Cartesian vectors and tensors have been used, so that the spatial coordinates x, y, z are denoted by $i = 1, 2, 3$, so that for $i \equiv y$ is $g_i = g = -\partial\varphi/\partial y$ (φ is the gravitational potential), and otherwise is $g_i = 0$. Besides, v_{ni} , ρ_n , and p_n correspond to the i^{th} component of the velocity, to the density and to the pressure, respectively. In addition, $\sigma_{ik}^{(n)}$ is the deviatoric part of the stress tensor $\Sigma_{ik}^{(n)} = -p_n \delta_{ik} + \sigma_{ik}^{(n)}$ of the medium n (δ_{ik} is the Kronecker δ). For the sake of convenience in the presentation, vector and index notation will be interchanged when suitable. Moreover, the material derivative of any magnitude M is

$$\frac{dM}{dt} = \frac{\partial M}{\partial t} + v_{ni} \frac{\partial M}{\partial x_i}. \quad (3)$$

As the first step, we linearize the conservation equations in the usual manner such as it was done in Refs. [47,54]. For this, every magnitude M is written as $M = M_0 + \delta M$ where M_0 is the equilibrium value of M and $\delta M \ll M_0$ is the

corresponding perturbation. Thus, from Eqs. (1) and (2) we get:

$$\frac{\partial(\delta v_{ni})}{\partial x_i} = 0, \quad (4)$$

$$\rho_n \frac{\partial(\delta v_{ni})}{\partial t} = -\frac{\partial(\delta p_n + \rho_n \delta \varphi_n)}{\partial x_i} + \frac{\partial S_{ik}^{(n)}}{\partial x_k}, \quad (5)$$

where incompressible perturbations ($\delta \rho_n = 0$) have been assumed, and $\delta \sigma_{ik}^{(n)} \equiv S_{ik}^{(n)}$.

Hereafter, we follow a procedure analogous to the one adopted in Ref. [54] for the RTI in accelerated solid slabs (with a free surface). Thus, we take $S_{ik}^{(1)} = 0$ for the ideal medium ($n = 1$), and we use the nonlinear Prandtl-Reuss model for the elastic-plastic slab in which the solid behaves like a perfectly elastic Hookean (linear) solid for the smaller strains and it behaves like a rigid-plastic solid when the stress overcome the elastic limit Y [42,43]. Therefore, in the elastic phase, we can write

$$\frac{\partial S_{ik}^{(2)}}{\partial t} = 2G\dot{e}_{ik}; \quad e_{ik} = \frac{1}{2} \left[\frac{\partial \eta_{2i}}{\partial x_k} + \frac{\partial \eta_{2k}}{\partial x_i} \right], \quad (6)$$

where the upper dot indicates time derivative and e_{ik} is the strain tensor, and η_{ni} are the components of the displacement vector $\boldsymbol{\eta}_n$ ($\dot{\boldsymbol{\eta}}_n = \delta \mathbf{v}_n$). For the plastic phase we write [22,42,43]

$$S_{ik}^{(2)} = \sqrt{\frac{2}{3}} \frac{\dot{e}_{ik}}{\|\dot{e}_{ik}\|} Y. \quad (7)$$

As it was already discussed in Ref. [54], the usual von Mises criterion accounting for the onset of plastic flow not necessarily describes the transition from the instability regime controlled by the elasticity to the one controlled by the plasticity. In fact, we must take into account the fact pointed out by Drucker [39,40] that for the instability of the system, it is not enough to marginally overcome the phase of contained plastic flow given by the von Mises criterion, but it must achieve a subsequent phase of unrestricted plastic flow. This is because during the phase of contained plastic flow the elasticity still plays a major role and it must be considered as a part of the previous elastic phase [55]. This procedure, developed in the analysis of soil plasticity is of particular significance for RTI in which the onset of plastic flow starts on the interface, where deformation is a maximum, and then, it progresses towards the slab interior. Since in RTI we have to deal with the average motion of a region affected by the instability, which extends up to a distance of the order of $d = \min \{h, k^{-1}\}$ from the interface, RTI is not expected to be sensitive to the onset of the plastic flow until it has affected the entire region with thickness of the order of d [42].

As it was shown in Refs. [47,54], the determination of the stability regions in terms of the initial amplitude and wavelength of the perturbations, requires one to know the time evolution of the perturbation amplitude along the successive elastic and plastic phases, which at the same time depends on the asymptotic growth rates given by the corresponding dispersion relations in each regime.

A. Instability analysis in the elastic phase

1. Displacement field

To derive the differential equation for the evolution of the perturbations on the interface ($y = 0$) we follow the procedure already described in Refs. [47,54] that we briefly summarize here, which consists in applying the Helmholtz decomposition to the displacement field:

$$\boldsymbol{\eta}_2 = \nabla \phi_2 + \nabla \times (\psi_2 \mathbf{e}_z), \quad (8)$$

where ϕ_2 and $\boldsymbol{\psi}_2 = \psi_2 \mathbf{e}_z$ are the Lamé scalar and vector potentials functions, respectively. Introducing Eq. (8) into Eqs. (4) and (5), we obtain the following system for the potential functions:

$$\nabla^2 \phi_n = 0, \quad (9)$$

$$\nabla \left(\frac{\partial^2 \phi_n}{\partial t^2} + \frac{\delta p_n}{\rho_n} + \delta \varphi_n \right) + \nabla \times \left[\left(\frac{\partial^2 \psi_n}{\partial t^2} - \frac{G}{\rho_n} \nabla^2 (\psi_n \mathbf{e}_z) \right) \right] = 0, \quad (10)$$

where, since the semi-infinite medium in the region $y \geq 0$ is considered to be ideal, we have $\psi_1 = 0$. As it is known, the vector potential in the Helmholtz's decomposition introduces a degree of freedom that allows for splitting Eq. (10) into two equations for the scalar and the vector potentials, respectively, through the choice of an adequate gauge [56–58]. Then, by adopting the Bernoulli gauge [56] the potentials ϕ_n and $\boldsymbol{\psi}_2$ can be chosen for satisfying the following equations:

$$\rho_n \frac{\partial^2 \phi_n}{\partial t^2} + \delta p_n - \rho_n \delta \varphi = 0, \quad (11)$$

$$\rho_2 \frac{\partial^2 \psi_2}{\partial t^2} = G \nabla^2 \psi_2. \quad (12)$$

Therefore, considering 2D perturbations and solving Eqs. (9) and (12) in the usual manner by separation of variables, we find that the solutions are, respectively, of the form $\phi_{2i} = F_\phi(t) \exp(\pm ky) \exp(\pm ikx)$, and $\psi_{2i} = F_\psi(t) \exp(\pm ly) \exp(\pm ikx)$. Then, we write the general expressions of the potential functions for the elastic medium in the following convenient form [47,54]:

$$\phi_2 = \frac{a \cosh ky + b \cosh k(h+y)}{\sinh kh} \sin kx, \quad (13)$$

$$\psi_2 = \frac{c \sinh ly + d \sinh \ell(h+y)}{\sinh \ell h} \cos kx, \quad (14)$$

where $k = 2\pi/\lambda$ is the perturbation wave number,

$$\ell = \sqrt{k^2 + \frac{\gamma_{ei}^2 \rho_2}{G}}, \quad (15)$$

and a, b, c and d are time functions such that

$$a \propto b \propto c \propto d \propto F(t) = \sum_i Q_i e^{\gamma_{ei} t}, \quad (16)$$

where $F(t) \propto F_\phi(t) \propto F_\psi(t)$, Q_i are constants, and γ_{ei} are all the possible solutions of the dispersion relation that will be determined by the boundary conditions on the interface and on the rigid wall. In addition, the potential ϕ_1 associated to

the displacement field in the region $y \geq 0$ turns out ($\psi_1 = 0$) to be

$$\phi_1 = a_1 e^{-ky} \sin kx, \quad a_1 \propto F(t). \quad (17)$$

2. Boundary conditions and dispersion relation

Adequate boundary conditions on the interface ($y = 0$) and on the rigid wall ($y = -h$) must be imposed to determine a, b, c, d and a_1 , and to find the values of the growth rate γ_{ei} .

From the continuity conditions of the tangential and normal stresses at $y = 0$ we get

$$S_{xy}^{(2)}(0) = 0, \quad (18)$$

$$-\delta p_1(0) = -\delta p_2(0) + S_{yy}^{(2)}(0), \quad (19)$$

where δp_n ($n = 1, 2$) are given by Eq. (11). And from the continuity of the normal velocity at $y = 0$, we have

$$\delta v_{1y}(0) = \delta v_{2y}(0) = \dot{\eta}(x, t), \quad (20)$$

where

$$\eta(x, t) = \eta_{2y}(0) = \xi(t) \sin kx. \quad (21)$$

Besides, the rigid wall boundary condition requires that the velocity at $y = -h$ be zero:

$$\delta v_{2x}(-h) = \delta v_{2y}(-h) = 0. \quad (22)$$

The previous boundary conditions constitute a set of linear equations from which we can obtain

$$\dot{a}_1 = -(\dot{b} + \dot{d}), \quad (23)$$

$$\dot{c} = -\dot{a}, \quad \dot{d} = -\frac{2k^2}{\ell^2 + k^2} \dot{b}, \quad (24)$$

$$\begin{aligned} &\dot{a}(k \coth kh - \ell \coth \ell h) \\ &+ \dot{b} \left[\frac{k}{\sinh kh} - \frac{2\ell k^2}{(\ell^2 + k^2) \sinh \ell h} \right] = 0, \end{aligned} \quad (25)$$

$$k\dot{b} = \frac{\ell^2 + k^2}{\ell^2 - k^2} \dot{\xi}. \quad (26)$$

Moreover, from Eq. (19) we get

$$\begin{aligned} &\frac{\rho_2}{k} \ddot{\xi} \left(\coth kh - \frac{F}{\sinh kh} \right) \\ &+ \frac{2kG\ddot{\xi}}{\gamma_{ei}^2} \left(\coth kh - \frac{F}{\sinh kh} \right) + C_0 \\ &+ 2kG(\xi - \xi_0) \frac{\ell^2 + k^2}{\ell^2 - k^2} \left(\coth kh - \frac{F}{\sinh kh} \right) \\ &+ \frac{\ell F}{k \sinh \ell h} - \frac{2\ell k}{\ell^2 + k^2} \coth \ell h \\ &= \rho_2 g \xi - \frac{\rho_1}{k} (\ddot{\xi} + k g \xi), \end{aligned} \quad (27)$$

where we have introduced the constant C_0 to take into account that the potential function in Eqs. (13) is defined to less than an arbitrary function of time and, using Eq. (15), we have rewritten Eq. (26):

$$\ddot{b} = \frac{\ddot{\xi}}{k} + \frac{\xi}{k} \frac{2k^2 G}{\rho_2 \gamma_{ei}^2}. \quad (28)$$

Moreover, $F = -\dot{a}/b$ is given by Eq. (25):

$$F = \frac{k}{\ell^2 + k^2} \frac{(\ell^2 + k^2) \operatorname{csch} kh - 2k\ell \operatorname{csch} \ell h}{k \coth kh - \ell \coth \ell h}. \quad (29)$$

In addition, in performing the integration of Eq. (6), we have considered that the solid slab is initially under stress free conditions. Thus, it turns out

$$\ddot{\xi}(\rho_1 + \rho_2 \coth kh) + k S_{ye}(0) = (\rho_2 - \rho_1) k g \xi, \quad (30)$$

where

$$\begin{aligned} S_{ye}(0) = 2kG \left\{ \frac{\ddot{\xi} - \ddot{\xi}_0}{\gamma_{ei}^2} \left[\coth kh - \frac{(\ell^2 + k^2)F}{2k^2 \sinh kh} \right] \right. \\ \left. + (\xi - \xi_0) \frac{\ell^2 + k^2}{\ell^2 - k^2} \left(\coth kh - \frac{F}{\sinh kh} \right) \right. \\ \left. + \frac{\ell F}{k \sinh \ell h} - \frac{2\ell k}{\ell^2 + k^2} \coth \ell h \right\}, \end{aligned} \quad (31)$$

where $\ddot{\xi}_0 = \ddot{\xi}(0)$. In writing Eq. (31) we have further considered that the displacement field $\eta(x, y, t)$ must be irrotational at $t = 0$ since vorticity is considered to be created by the elasticity effects at $t > 0$ ($\psi_2(t = 0) = 0$). Therefore, all the terms proportional to the shear modulus G must vanish at $t = 0$. Thus, the expression for S_{ye} in Eq. (31) includes a dynamical component given by the first term containing the acceleration increment $\ddot{\xi} - \ddot{\xi}_0$, which will contribute to the total loading leading to plastic flow.

In addition, the following initial conditions must be considered (at $t = 0$):

$$\xi(0) = \xi_0, \quad \dot{\xi}(0) = 0. \quad (32)$$

To solve the differential equation given by Eq. (30), we construct the general solution in the usual manner by postulating an exponential solution of the form $\xi \propto e^{\gamma_{ei} t}$ for the homogeneous part of the equation, and then adding a particular solution of the complete equation. Thus, by introducing such an exponential solution into the homogeneous part of Eq. (30), the dispersion relation for the asymptotic growth rate for the rigid wall case is obtained:

$$\begin{aligned} &\kappa(2\kappa^2 + \sigma^2)^2 + 4\kappa^3(\kappa^2 + \sigma^2) - [4\kappa^4 + (2\kappa^2 + \sigma^2)^2] \\ &\times \sqrt{\kappa^2 + \sigma^2} \coth \alpha \kappa \coth \alpha \sqrt{\kappa^2 + \sigma^2} \\ &+ 4\kappa^2(2\kappa^2 + \sigma^2) \sqrt{\kappa^2 + \sigma^2} \operatorname{csch} \alpha \kappa \operatorname{csch} \alpha \sqrt{\kappa^2 + \sigma^2} \\ &- \sigma^2 \left[\kappa - \frac{1 - A_T}{1 + A_T} (\kappa + \sigma^2) \right] (\kappa \coth \alpha \kappa \\ &- \sqrt{\kappa^2 + \sigma^2} \coth \alpha \sqrt{\kappa^2 + \sigma^2}) = 0, \end{aligned} \quad (33)$$

where we have used the following definitions for the dimensionless magnitudes:

$$\begin{aligned} \kappa &= \frac{k}{k_0}; \quad \sigma = \frac{\gamma_{ei}}{\sqrt{k_0 g}}; \quad k_0 = \frac{\rho_2 g}{G}, \\ \alpha &= \frac{\rho_2 g h}{G}; \quad A_T = \frac{\rho_2 - \rho_1}{\rho_2 + \rho_1}, \end{aligned} \quad (34)$$

As in the dispersion relation for the instability of accelerated solid slabs, Eq.(33) is a transcendental equation for σ^2 as a function of κ , with α and A_T as parameters, and σ^2 is always a real number [47,54]. Such an equation has a

unique real and positive root when the slab is unstable (for $\kappa_{cL} \leq \kappa \leq \kappa_{cH}$, where κ_{cL} and κ_{cH} are, respectively, the lower and the higher dimensionless cut-off wave numbers for which $\sigma = 0$). A graphical representation of σ^2 as a function of κ is given by Mora *et al.* [49] for the particular case with $A_T = 1$ and for different values of the parameter α , but with different definitions of the dimensionless magnitudes.

As we will see later, for our present purposes we are interested in the stable solutions of Eq. (33) corresponding to the cases when $-\Omega^2 \equiv \sigma^2 < 0$, which occur for $\kappa \leq \kappa_{cL}$ and $\kappa \geq \kappa_{cH}$, or below the threshold $2A_T\alpha/(1+A_T) \leq 6.223$ for which no cut-off wave number exists. In particular, when $\kappa \geq \kappa_{cH}$ Eq. (33) yields an infinite number of roots resulting from the divergence of the dispersion relation to infinity when $\alpha\sqrt{\kappa^2 - \Omega^2} = im\pi$, where m is an integer number [46,54]. In such a case we have

$$\Omega^2 = \kappa^2 + \frac{m^2\pi^2}{\alpha^2}. \quad (35)$$

Therefore, there is a root in between successive asymptotes for which $\Omega^2 \geq \kappa^2$. In addition, there is another root for which $\Omega^2 < \kappa^2$ that constitutes the smallest value of Ω^2 . As a consequence, in the stable ranges of κ , the perturbation amplitude at the interface consists, in general, of a multimodal oscillation containing an infinite number of frequencies corresponding to these infinite roots of the dispersion relation [46,54,56].

The lowest dimensionless oscillation frequency Ω as a function of the dimensionless perturbation wave number κ is shown in Fig. 2 for the stable cases ($\Omega^2 > 0$), for two different values of the Atwood number ($A_T = 1$ and $A_T = 0.4$) and for different values of the parameter α . In the limit $\kappa \rightarrow \infty$, we can see from the numerical solutions of the dispersion relation that it is $\Omega \rightarrow r\kappa$ ($r \approx 0.9$ to 0.96) almost independently of the values of A_T and α . In the opposite limit of $\kappa \rightarrow 0$, the lowest frequency turns out to be $\alpha\Omega(\kappa=0) = \pi/2$ for any value of A_T . The latter can be easily obtained analytically by noticing that, in the limit $\kappa \rightarrow 0$, the third term in Eq. (33) becomes the dominant one.

On the other hand, the unstable region between the lower and the higher cut-off wave numbers, in which $\Omega^2 < 0$, increases with the dimensionless slab thickness α and, in the limit $\alpha \rightarrow \infty$, it is $\kappa_{cL} \rightarrow 0$, thus retrieving the semi-infinite case for elastic RTI [48]. Moreover, when the slab thickness is below the threshold ($2A_T\alpha/(1+A_T) \leq 6.223$), curves a) and b) in Fig. 2, it is $\Omega^2 > 0$ for all the perturbation wave numbers, so that the slab is elastically stable. Besides, we can see that the existence of a lighter medium beneath the slab ($A_T < 1$) enhances the stability of the system such as it could be expected.

These results are better understood by looking at the conditions for marginal stability in the elastic regime already studied by Mora *et al.* [49]. Such conditions correspond to $\sigma^2 = 0$ in Eq. (33) and are easily determined after a first-order Taylor development of the terms of the form $\coth \ell h$ and $\operatorname{csch} \ell h$ in Eq. (33):

$$\begin{aligned} \coth \ell h &\approx \coth kh - \frac{(\ell - k)h}{(\sinh kh)^2}, \\ \operatorname{csch} \ell h &\approx \operatorname{csch} kh - \frac{(\ell - k)h}{(\sinh kh)^2} \cosh kh. \end{aligned} \quad (36)$$

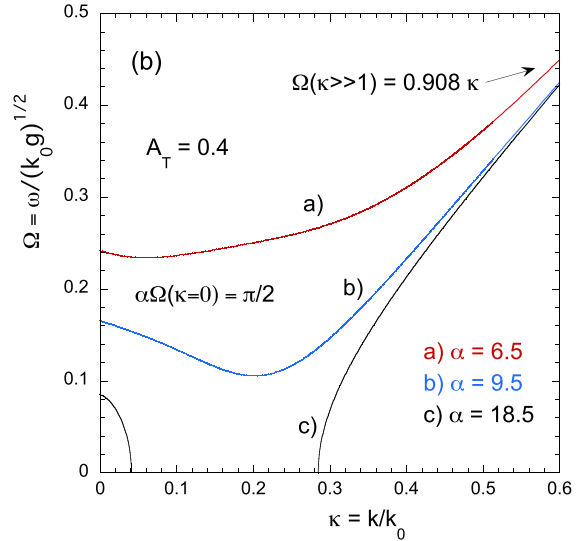
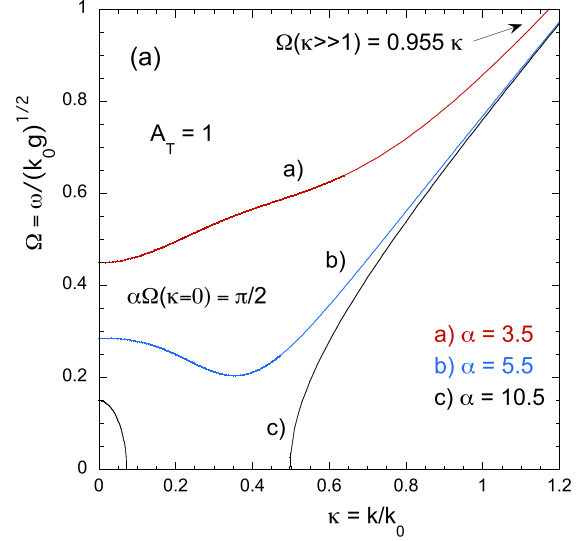


FIG. 2. Dimensionless oscillation frequency Ω for the stable regimes as a function of the dimensionless perturbation wavenumber κ , for $A_T = 1$ (a), and for $A_T = 0.4$ (b), and for different values of the dimensionless slab thickness α .

Thus, after some algebra, we get

$$\frac{2A_T}{1+A_T}\alpha = \frac{2w(2w^2 + \cosh 2w + 1)}{\sinh 2w - 2w}, \quad (37)$$

($w = k_c h$) which is the straightforward generalization for arbitrary Atwood number of the result presented in Refs. [49,50] in absence of interfacial surface tension. The graphical representation of the previous equation is shown in Fig. 3 where it can be seen that for $2A_T\alpha/(1+A_T) \approx 6.223$ there is a threshold below which the interface becomes elastically stable for any perturbation wave number. Above such a threshold value, the interface is unstable for a finite range of κ values ($\kappa_{cL} \leq \kappa \leq \kappa_{cH}$).

The existence of two cut-off wave numbers when the elastic slab is in contact with a rigid wall contrasts with the case of accelerated elastic slabs (free surface), in which there is only one cut-off wave number κ_c and, therefore, the slab is

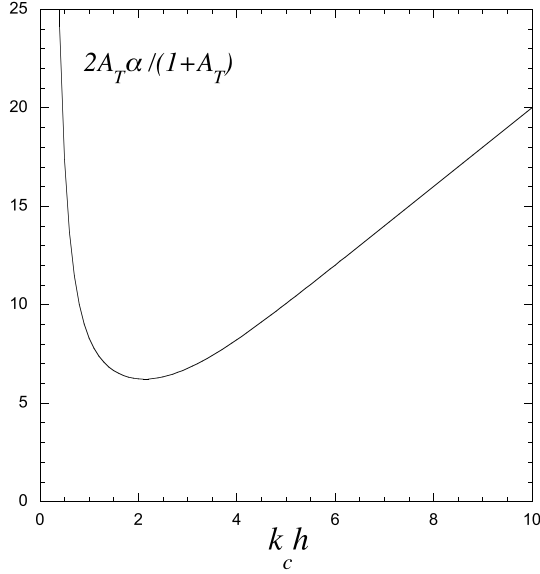


FIG. 3. Normalized dimensionless slab thickness $2A_T\alpha/(1+A_T)$ as a function of the cutoff wave number $k_c h$.

always unstable for $0 \leq \kappa \leq \kappa_c$ and any value of A_T , provided that the dimensionless thickness α is above a threshold value ($\alpha > 2(1 - A_T)/A_T$) [54]. Moreover, it also differs from any other case of RTI involving fluids in contact with a rigid wall (either ideal or viscous). This indicates that the existence of the lower cut-off wave number κ_{cL} must be a result of the unique combination of the stabilization effects provided by the elasticity and by the contact with the rigid wall. A similar behavior was found in Refs. [10,11] for the case of an elastic slab with a very high conductivity and in the presence of a sufficiently strong horizontal magnetic field on the top of the slab. In such case, the appearance of the lower cut-off is a consequence of the reduction of the perturbed vertical velocity by the magnetic field, and the no slip conditions seems to be irrelevant for the existence of this lower cutoff. A further discussion on the significance of these two cut-off wave numbers can be found in Refs. [49–51]

B. Instability analysis in the plastic phase

In the same manner as in the case of accelerated solid slabs [54], the analysis of the instability in the plastic regime is performed by assuming classical plasticity. Therefore, the displacement field in such a phase must be irrotational [59], and the Lamé potentials are given by Eqs. (13) and (17), for the solid and for the ideal medium, respectively ($\psi_2 = 0$). Besides, the boundary conditions given by Eqs. (18) to (21) must be still satisfied.

As it was previously mentioned, although an intermediate stage exists between the purely elastic phase and the late phase of unrestricted flow (plastic collapse) [39,40], it can be assimilated to the elastic regime and it can be considered that the evolution of the RTI after the initial elastic phase is followed by the late phase of plastic collapse [55]. Then, as it was already shown for the case of accelerated solid slabs [54], we can describe the plastic phase evolution of the instability

with the methods of the limit analysis discussed in the book by Chen [55], such as it was proposed by Drucker, by taking the average of Eq. (19) over half a wavelength and considering the sinusoidal perturbation at the interface like a set of bumps of height twice the perturbation amplitude [39,40]. Therefore Eq. (19) turns out to be

$$\ddot{\xi}(\rho_1 + \rho_2 \coth kh) + kS_{yp}(0) = (\rho_2 - \rho_1)gk\xi, \quad (38)$$

where $S_{yp}(0) \approx 2Y$ and, following Drucker, we have considered that the unrestricted plastic flow occurs when the loading force L at the bottom level of the interface (the valleys) averaged over half a wavelength is $L = (1 + \pi/2)Y(\lambda/2)$. In addition, in averaging Eq. (19) we have considered that $(2/k) \int_0^\pi \sin u \, du = (4/\pi)(\lambda/2)$, and that $(1 + \pi/2)(\pi/4) \approx 2$ [39,40,54,55]. This procedure is equivalent to considering a somewhat higher value of the yield strength Y in Eq. (7).

Once again, the general solution of Eq. (38) can be written as the solution of the homogeneous equation plus a particular one, where the solutions for the homogeneous equations are found by proposing an exponential form: $\xi_p \propto e^{\gamma_{pi}}$; where now γ_{pi} corresponds to the growth rate for the plastic phase and it is determined by the solutions of the dispersion relation for the ideal fluid slab case [60]:

$$\sigma_p^2 = \frac{2A_T\kappa}{1 - A_T + (1 + A_T) \coth \alpha\kappa}, \quad (39)$$

where $\sigma_p = \gamma_{pi}/\sqrt{k_0g}$ and the dimensionless magnitudes defined in Eq. (34) have been used.

III. STABILITY BOUNDARIES

A. Average evolution of the perturbation amplitudes

For the system being stable, the necessary condition is that it must be stable during the elastic phase [42,43,54]. Then, as shown in Fig. 3, the perturbation wave number throughout such a phase must be $\kappa \leq \kappa_{cL}$ or $\kappa \geq \kappa_{cH}$, or $2A_T\alpha/(1+A_T) \leq 6.223$ ($-\Omega^2 \equiv \sigma^2 < 0$).

Since in such a case Eq. (33) has an infinite number of roots, the general solutions of the homogeneous parts of Eq. (30) is given by the linear combination of the solutions corresponding to each one of these roots, being extended to infinity the summation in Eq. (16) and resulting the general solution in a multimodal oscillation. However, it can be considered that in the stable regime, the perturbation amplitude at the interface can be written as the sum of an average oscillation determined by the lowest frequency plus infinite superimposed oscillation modes of higher frequencies. Therefore, we will assume that it is this average amplitude of the perturbation corresponding to the minimum frequency, the one that determines the evolution of the instability that determines the stability boundaries [54].

Then, during the elastic phase in the stable regime, the average amplitude at the interface is obtained by solving the differential equation given by Eq. (27) in the usual manner by proposing a sinusoidal solution for the homogeneous part and adding to it a particular solution, and considering that the oscillation takes place with average frequency. Then, with the

initial conditions given by Eq. (32), we get

$$z - 1 = (z_{1e} - 1)(1 - \cos \Omega \tau), \quad (40)$$

where Ω corresponds to the lowest oscillation frequency given by Eq. (33), and the following dimensionless magnitudes has been defined:

$$z = \frac{\xi}{\xi_0}; \quad \tau = t\sqrt{k_0g},$$

$$\Omega = i\sigma = \frac{\omega_e}{\sqrt{k_0g}}; \quad z_{1e} - 1 = \frac{\ddot{\xi}_0}{\xi_0\omega_e^2}. \quad (41)$$

Moreover, the initial acceleration $\ddot{\xi}_0$ can be obtained by evaluating Eq. (30) at $t = 0$ ($S_{ye}(0, t = 0) = 0$):

$$\frac{\ddot{\xi}_0}{\xi_0\omega_e^2} = \frac{\sigma_p^2}{\Omega^2}. \quad (42)$$

On the other hand, the transition from the elastic to the plastic regime will occur at the transition time t_T , when the average perturbation amplitude in the elastic phase ($t \leq t_T$) achieves the boundary of unrestricted plastic flow, which will take place before the amplitude reaches an absolute maximum. In such a case, for $t > t_T$ the stability of the system depends on the amplitude at t_T and on the plastic flow condition.

Once in the plastic phase ($t \geq t_T$), the evolution of the perturbation amplitude is mainly ruled by the growth rate σ_p , given by Eq. (39):

$$z = \frac{1 + A_T}{2A_T} \frac{1}{\xi^*} + K_1 e^{\sigma_p \tau} + K_2 e^{-\sigma_p \tau}, \quad (43)$$

where the first term is a particular solution of Eq. (38) in its dimensionless form, and the dimensionless initial amplitude is defined as follows:

$$\xi^* = \frac{\rho_2 g \xi_0}{2Y}. \quad (44)$$

To obtain the constants K_1 and K_2 we impose to Eq. (40) (for $t \leq t_T$) and Eq. (43) (for $t \geq t_T$) the matching conditions at $t = t_T$:

$$\xi_e(t = t_T) = \xi_p(t = t_T) = \xi_T, \quad (45)$$

$$\dot{\xi}_e(t = t_T) = \dot{\xi}_p(t = t_T) = \dot{\xi}_T, \quad (46)$$

$$S_{ye}(0, t = t_T) = S_{yp}(0, t = t_T), \quad (47)$$

where subscripts e and p denote, respectively, the amplitude ξ in the elastic and plastic regimes, ξ_T is the amplitude at the transition time, S_{ye} is given by Eq. (31), and $S_{yp} = 2Y$. Besides, from Eqs. (38) and (40) we can write:

$$\ddot{\xi}_T - \ddot{\xi}_0 = -\omega_e^2(\xi_T - \xi_0). \quad (48)$$

In addition, Eq. (47) can be written in dimensionless form as follows:

$$(z_T - 1) \frac{(A_1 A_2 - C_1 C_2)}{C_1} = \frac{\lambda^*}{\xi^*}, \quad (49)$$

where definitions given by Eqs. (41) and (44) have been used, $z_T = z(t = t_T)$ and the following dimensionless magnitudes have been introduced:

$$\lambda^* = \frac{\rho_2 g \lambda}{4\pi G} = \frac{1}{2\kappa}, \quad (50)$$

$$A_1 = \kappa \operatorname{csch} \alpha \kappa - \frac{2\kappa^2 \sqrt{\kappa^2 - \Omega^2}}{2\kappa^2 - \Omega^2} \operatorname{csch} \alpha \sqrt{\kappa^2 - \Omega^2}, \quad (51)$$

$$A_2 = \frac{(2\kappa^2 - \Omega^2)^2}{2\kappa^2 \Omega^2} (\operatorname{csch} \alpha \kappa - \frac{2\kappa \sqrt{\kappa^2 - \Omega^2}}{2\kappa^2 - \Omega^2} \operatorname{csch} \alpha \sqrt{\kappa^2 - \Omega^2}), \quad (52)$$

$$C_1 = \kappa \coth \alpha \kappa - \sqrt{\kappa^2 - \Omega^2} \coth \alpha \sqrt{\kappa^2 - \Omega^2}, \quad (53)$$

$$C_2 = \frac{2(\kappa^2 - \Omega^2)}{\Omega^2} (\coth \alpha \kappa - \frac{\kappa}{\sqrt{\kappa^2 - \Omega^2}} \coth \alpha \sqrt{\kappa^2 - \Omega^2}), \quad (54)$$

Now, from Eqs. (40) and (49) the transition time t_T turns out to be

$$\cos \Omega \tau_T = 1 - \frac{1}{(z_{1e} - 1) \xi^*} \left[\frac{C_1}{(A_1 A_2 - C_1 C_2)} \right], \quad (55)$$

where $\tau_T = t_T/t_0$ is the dimensionless time for the transition to the plastic regime.

Finally, constants K_1 and K_2 in Eq. (43) can be calculated from the matching conditions in Eqs. (45) and (46):

$$1 + \frac{\lambda^*}{\xi^*} \frac{C_1}{(A_1 A_2 - C_1 C_2)} = \frac{1 + A_T}{2A_T} \frac{1}{\xi^*} + K_1 e^{\sigma_p \tau_T} + K_2 e^{-\sigma_p \tau_T}, \quad (56)$$

$$(z_1 - 1) \Omega \sin \Omega \tau_T = \sigma_p (K_1 e^{\sigma_p \tau_T} - K_2 e^{-\sigma_p \tau_T}). \quad (57)$$

and by solving for K_1 and K_2 :

$$2K_2 e^{-\sigma_p \tau_T} = 1 + \frac{\lambda^*}{\xi^*} \frac{C_1}{(A_1 A_2 - C_1 C_2)} - \frac{1 + A_T}{2A_T} \frac{1}{\xi^*} - (z_1 - 1) \frac{\Omega}{\sigma_{p1}} \sin \Omega \tau_T, \quad (58)$$

$$2K_1 e^{\sigma_p \tau_T} = 1 + \frac{\lambda^*}{\xi^*} \frac{C_1}{(A_1 A_2 - C_1 C_2)} - \frac{1 + A_T}{2A_T} \frac{1}{\xi^*} + (z_1 - 1) \frac{\Omega}{\sigma_{p1}} \sin \Omega \tau_T. \quad (59)$$

B. Stability boundaries

The interface will be stable provided that the average amplitude ξ reaches an absolute maximum at a certain time $t = t_m \geq t_T$ Refs. [42,43,54] so, it must be $\dot{\xi}(t_m) = 0$ and $\ddot{\xi}(t_m) \leq 0$ if the slab is stable. Therefore, stability boundaries will be determined by the following conditions for marginal stability:

$$\dot{z}(\tau_m) = 0; \quad \ddot{z}(\tau_m) = 0; \quad (\tau_m \geq \tau_T). \quad (60)$$

These conditions can only be satisfied in the regime when the system is stable in the purely elastic phase ($\kappa \leq \kappa_{cL}$ or $\kappa \geq \kappa_{cH}$, or $2A_T \alpha / (1 + A_T) \leq 6.223$) [42,43,54]. Therefore, we

apply the previous marginal stability conditions to the plastic regime evolution described by Eq. (43) (with K_1 and K_2 given by Eqs. (58) and (59), respectively). Since Eq. (60) will only be satisfied when $K_2 = 0$, the curve of marginal stability turns out to be

$$1 + \frac{1}{\xi^*} \left[\frac{\lambda^* C_1}{(A_1 A_2 - C_1 C_2)} - \frac{1 + A_T}{2A_T} \right] = \frac{\sigma_p}{\Omega} \sin \Omega \tau_T, \quad (61)$$

where by using Eqs. (41) and (42) we have written

$$(z_{1e} - 1) = \frac{\sigma_p^2}{\Omega^2}. \quad (62)$$

In addition, from Eq. (55) it turns out that

$$\sin \Omega \tau_T = \sqrt{1 - \left[1 - \frac{\lambda^* \Omega^2}{\xi^* \sigma_p^2} \frac{C_1}{(A_1 A_2 - C_1 C_2)} \right]^2}, \quad (63)$$

where Eq. (50) has to be used to write the functions $A_i = A_i(\lambda^*)$ and $C_i = C_i(\lambda^*)$ ($i = 1, 2$) given by Eqs. (51)–(54) in terms of λ^* . It may be relevant to notice that the marginal stability conditions in Eq. (60) also lead to $K_1 = 0$ and it also yields Eq. (64). However, it is worth remarking that these values of K_1 and K_2 are taken only on the curve of marginal stability and that, in general, they are not null.

Introducing Eq. (62) into Eq. (61) and reordering terms, the following quadratic equation for $\xi^* = \xi^*(\lambda^*)$ can be obtained, with α and A_T as parameters, which completely determines the stability boundaries in the plane (ξ^*, λ^*) :

$$\xi^{*2} + F_1(\lambda^*)\xi^* + F_2(\lambda^*) = 0, \quad (64)$$

where

$$F_1 = \frac{1 + A_T}{2A_T}, \quad (65)$$

$$F_2(\lambda^*) = \left(H - \frac{1 + A_T}{2A_T} \right)^2 + \left(\frac{H\Omega}{\sigma_p} \right)^2, \quad (66)$$

and

$$H = \frac{\lambda^* C_1}{A_1 A_2 - C_1 C_2}, \quad (67)$$

where Eq. (39) gives σ_p , and Ω corresponds to the smallest root of Eq. (33) for $\kappa \leq \kappa_{cL}$ or $\kappa \geq \kappa_{cH}$, when $2A_T\alpha/(1 + A_T) \geq 6.223$, or for any value of κ when $2A_T\alpha/(1 + A_T) \leq 6.223$.

C. Plastic flow boundaries

In order to obtain the boundary for the elastic-plastic (EP) transition we require that the transition amplitude z_T be reached when in the elastic regime the oscillation amplitude reaches its maximum value $z^{\max} = z_{1e}$. Thus, we have

$$z_{1e} - 1 = \frac{2\ddot{\xi} a_0}{\xi_0 \omega_e^2} = z_T - 1. \quad (68)$$

Therefore, from Eqs. (49) and (62) we obtain the dimensionless amplitude $\xi_{EP}^* = \rho_2 g \xi_{EP} / 2Y$, for which the transition from the elastic to the plastic regime occurs:

$$\xi_{EP}^* = \frac{1}{2} \left(\frac{\Omega}{\sigma_p} \right)^2 \frac{\lambda^* C_1}{(A_1 A_2 - C_1 C_2)}. \quad (69)$$

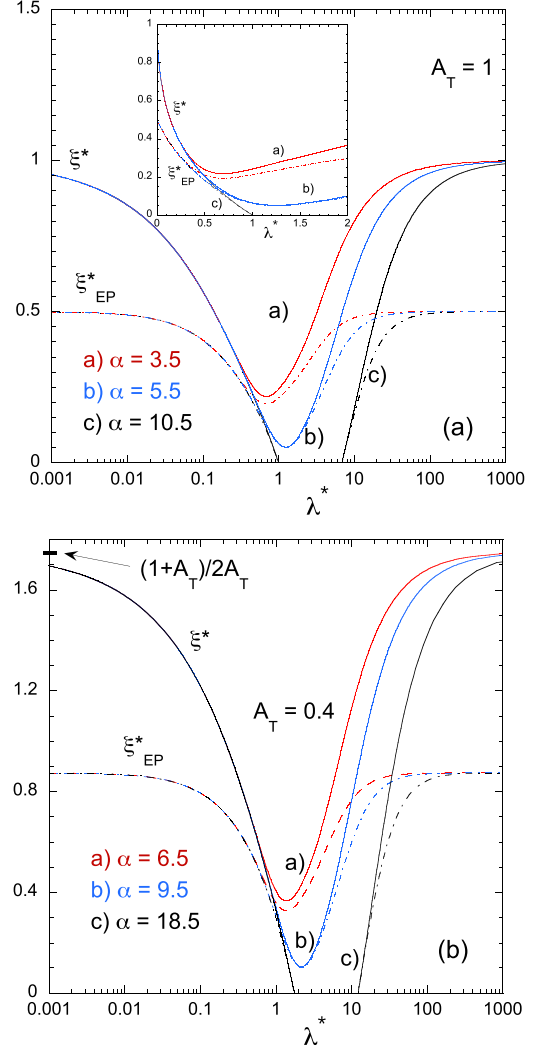


FIG. 4. Boundaries for stability ξ^* (full lines) and for the elastic-plastic transition ξ_{EP}^* (dotted lines) for $A_T = 1$ (a), and for $A_T = 0.4$ (b), and for different values of the dimensionless slab thickness α .

IV. RESULTS OF THE THEORY AND DISCUSSION

The stability boundary $\xi^*(\lambda^*)$ such as given by Eqs. (64)–(67), and the plastic flow boundary $\xi_{EP}^*(\lambda^*)$ given by Eq. (69), have been represented in Fig. 4 for $A_T = 1$ and $A_T = 0.4$ and for several values of the dimensionless slab thickness α .

In this figure we can see that the behavior of the system is qualitatively the same for the different values of A_T , and that the effect of the presence of the light medium beneath the slab is, as it could be expected, to enhance the range of perturbation amplitudes ξ^* for which the slab is stable. In particular, in the limits $\lambda^* \rightarrow 0$ and $\lambda^* \rightarrow \infty$, the stability boundary curves $\xi^*(\lambda^*)$ converge to the maximum value $\xi^{*\max} = (1 + A_T)/2A_T$, for any value of the dimensionless slab thickness α . The short wavelength limit would correspond to the Drucker criterion for an arbitrary Atwood number [39,40].

In addition, curves c) of Fig. 4 correspond to the cases in which α is above the threshold value $\alpha_0 = 6.223[2A_T/(1 + A_T)]$ shown in Fig. 3 [49,50], and the slab is unstable for

the perturbation wavelengths range that correlates with the wave numbers in between the two cutoffs for which the slab is already unstable in the early elastic phase (see Figs. 2 and 3). Therefore, in such a region the system will be unstable for any perturbation amplitude $\xi^* > 0$, provided that all the possible perturbation wavelengths are present in the system. Otherwise, for a given wavelength λ^* the required amplitude for instability must be above the corresponding curve $\xi^*(\lambda^*)$ for a given value of α . In particular, in the limit $\alpha \rightarrow \infty$, the lower cutoff $\kappa_{cL} \rightarrow 0$ and the semi-infinite case is recovered [42,43,54].

As α decreases and approaches the threshold value α_0 the distance between the two cut-off wavelengths reduces and both coincides when $\alpha = \alpha_0$. Then, for $\alpha < \alpha_0$ the slab is stable in the elastic phase, and a perturbation amplitude ξ^* larger than a minimum value $\xi_m^* > 0$ is required to make unstable the system [curves a) and b)]. This, as noticed above, is assuming that all the perturbation wavelengths are present in the system. In the limit $\alpha \rightarrow 0$, $\xi^* \rightarrow (1 + A_T)/2A_T$, and the stability is determined only by the initial perturbation amplitude.

On the other hand, similar tendencies are followed by the EP transition curves $\xi_{EP}^*(\lambda^*)$, being always below the $\xi^*(\lambda^*)$ curves, in concordance with previous results for accelerated solid slabs showing that, in general, plastic flow is a necessary but not a sufficient condition for instability [42,43,54]. We can also see that for any value of A_T , in the limits $\lambda^* \rightarrow 0$ and $\lambda^* \rightarrow \infty$, these curves converge to the maximum value $\xi_{EP}^{*\max} = (1 + A_T)/4A_T$, independently of α , being always half of the value $\xi^{*\max}$.

Besides, when $\alpha > \alpha_0$ the EP transition boundaries ξ_{EP}^* converge to the instability boundaries ξ^* as λ^* approaches the cut-off values from both sides, indicating that close to the cutoff the stable elastic region is practically nonexistent, though it becomes progressively wider at both sides of the cut-off wavelengths. When $\alpha < \alpha_0$ the EP boundaries still approach to the instability boundaries close to the minimum, but they gradually separate from each other for the lowest values of α . Such a behavior is expected because for $\alpha \rightarrow 0$, the minimum value ξ_{EPm}^* must become $\xi_{EPm}^* = \xi_m^*/2$. The inset in Fig. 4(a) shows the region close to $\lambda^* \sim 1$ in linear scale for more details.

A remarkable and not self-evident feature resulting from Fig. 4 is the approximate but very accurate scalings of the minimum value ξ_m^* of the dimensionless initial perturbation amplitude, and of the dimensionless perturbation wavelength λ_m^* at which it occurs, with the dimensionless slab thickness α . These parameters are relevant because in a real experiment, the system would become unstable once the initial perturbation amplitude overcomes this minimum ξ_m^* value, provided that the experiment contains a sufficiently wide range of perturbation wavelengths as for including λ_m^* .

These scalings cannot be inferred directly from the equations, but they are revealed by numerical calculations with an accuracy better than 4 %, and show that the quantities $2A_T\xi_m^*/(1 + A_T)$ and $2A_T\lambda_m^*/(1 + A_T)$ are universal functions of $2A_T\alpha/(1 + A_T)$ independently of the Atwood number, such as shown in Fig. 5.

Interestingly, such scalings allow for an interpretation of the experimental results recently reported by Maimouni *et al.* [52]. Indeed, the experiment deals with the situation in which

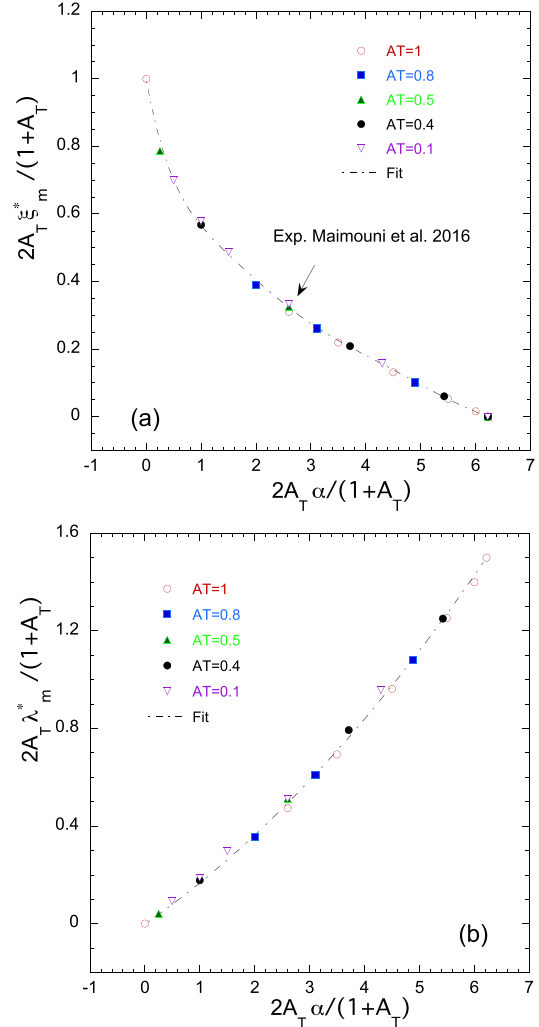


FIG. 5. Scaling laws for the normalized dimensionless minimum initial perturbation amplitude $2A_T\xi_m^*/(1 + A_T)$ (a), and for the corresponding perturbation wavelength $2A_T\lambda_m^*/(1 + A_T)$ (b), in terms of the normalized dimensionless slab thickness $2A_T\alpha/(1 + A_T)$.

the EP slab is the lighter medium placed at the bottom part in the experimental tank, but obviously it is entirely equivalent to the situation shown in Fig. 1. Therefore, it can be analyzed with the present theory. Thus, according to Fig. 5(a), for a given value of $2A_T\alpha/(1 + A_T) \equiv c_1$ there exists a unique value of $2A_T\xi_m^*/(1 + A_T) \equiv c_2$. From the main body of Fig. 3 in Ref. [52] we have $G \approx 0.225(\rho_2 - \rho_1)$ (G is in Pa and densities in kg/m^3), and with the parameters of the experiment ($g = 9.8 m/s^2$ and $h = 0.06 m$) we get $c_1 \approx 2.6$ as an average value for the whole set of experiments performed with different values of G and $\Delta\rho = \rho_2 - \rho_1$. According to Fig. 5(a), this value corresponds to $c_2 \approx 0.323$. Therefore, the results reported in the inset of Fig. 3 in Ref. [52] (for which it is $Y/\Delta\rho \approx 0.015$) would correspond to an average minimum initial amplitude of the perturbation $\xi_0 \approx 1 mm$. Certainly, this would be an average value for all the experiments since, for the nature of such experiments, the initial perturbation amplitude was not a controlled parameter. That is, for any individual experiment, a particular value of the initial

amplitude ξ_0 is determined by the experimental procedure, which at the same time determines a particular value of the slope value c_2 and, in virtue of the scaling in Fig. 5, it also determines the slope value c_1 . Therefore, the particular values of the average slopes in Fig. 3 of Ref. [52] are a consequence of the specific experimental procedure and they would result in a different way if such a procedure would have introduced a different average initial amplitude. Actually, for any particular experiment, the different values of c_1 and c_2 are quite evident from the Fig. 3 of Ref. [52].

As we have already mentioned, for the system being unstable for initial amplitudes just above the minimum value ξ_m^* , it is required that the perturbations wavelengths corresponding to $2A_T\lambda_m^*/(1+A_T)$ be present in the experiments. From Fig. 5(b) we find $2A_T\lambda_m^*/(1+A_T) \approx 0.49$ (for $c_1 \approx 2.6$), which corresponds to a perturbation wavelength $\lambda_m \approx 14$ cm. Since the experiments of Ref. [52] should contain all the perturbation wavelengths $\lambda \leq 2L$ (where L is the length of the experimental tank) the experimental results should not show any difference by changing the tanks length provided that $L \geq 7$ cm, such as it is reported in Ref. [52]. In this regard, it may be relevant to notice that validity of the linear theory requires $k\xi \ll 1$, and it will break for sufficiently small values of the perturbation wavelength λ . However, the extent of the wavelengths range in which linear theory is valid will depend on the particular conditions of the experiment. Namely, gravity acceleration, density contrast, perturbation initial amplitude, and thickness of the solid slab. For the particular case of the experiment reported in Ref. [52], in which the wavelength spectrum includes the minimum value $\lambda_m \sim 10$ cm, and for which we have estimated and initial perturbation amplitude $\xi_0 \sim 1$ mm, it turns out $\xi_0/\lambda < 0.01$ and, therefore, the conditions for the validity of the linear theory are very well satisfied.

In our interpretation of the experimental results of Ref. [52], we have taken into account the results of the creep test presented in that work, which shows that the elastic-plastic medium can be characterized by defined values of the shear modulus G and of the yield strength Y . However, the authors also presented the results of a penetration test which they considered to contrast with the previous ones. Such a penetration test was assumed to mimic the dynamics of the perturbation growth, and it was considered for providing an interpretation of the experimental results.

In our opinion, this penetration test has no clear relation with the dynamics of the perturbation growth and, in addition, its results can be interpreted compatibly with those of the creep test. In fact, as soon as the plate with a rounded edge is introduced into the elastic-plastic material, it acts as a blade that generates a high pressure on a small surface, which easily overcomes the material yield strength. Thus, plastic flow is induced in the region close to the edge practically from the very beginning of the penetration process. However, this process differs from the one that governs the dynamics of RTI, which is driven by the hydrostatic pressure arising as soon as a small perturbation is produced on the interface. Moreover, this pressure is proportional to the perturbation amplitude and it grows during the instability evolution leading, eventually, to local plastic flow when it overcomes the material yield strength. But, as it was previously discussed, the RTI regime

controlled by plasticity does not occurs until the plastic flow has affected an entire region of thickness $d = \min\{h, k^{-1}\}$ [19,20,42].

For concluding, it may be also relevant to mention that we cannot know the effects of sliding barrier place between the media in the experiment of Ref. [52], but we assume that it is removed in such a manner that the only effect is to create the initial spectrum of perturbation amplitudes and wavelengths. This is a plausible assumption provided that the time during which the generated shearing forces on the interface act on times longer than the characteristic time of growth of the instability. The good comparison of the present theory with the experimental results seems to support such an assumption.

V. CONCLUDING REMARKS

Following the methodological procedure developed in Ref. [54] we have extended the previous results for the RTI in accelerated elastic-plastic solid slabs, to the situation in which the slab is attached to a rigid wall. Thus, we intend to describe experiments with soft matter that can be performed in relatively small scale labs, compared with the HED matter experiments, but that share many common features and provide valuable physical insight that can be extrapolated to such larger scale experiments.

The previous conclusion that, in general, plastic flow is a necessary but not a sufficient condition for instability is retrieved. Differently than for the case of systems with a free surface (accelerated slabs), there exists a long wavelength stability region in which the required initial perturbation amplitude increases up a maximum $\xi^{*\max} = (1+A_T)/2A_T$, which is the same as for the short wavelength limit. In the intermediate region, the slab may be still stable but the required initial perturbation amplitude ξ^* reduces up to a minimum value ξ_m^* which becomes smaller as the dimensionless slab thickness α increases. And, for $\alpha > \alpha_0$ an unstable region for any value of $\xi^* > 0$ appears, that is bounded by two cut-off wavelengths that correlate with the cut-off wave numbers between which the system is elastically unstable.

Such a minimum initial perturbation amplitude, as well as the perturbation wavelength at which it occurs, follows the approximate but very accurate scaling laws represented in Fig. 5 that allows for an interpretation of the recent experiments reported in Ref. [52]. This fact reinforces the confidence in the theoretical approach also used for describing RTI under HED physics conditions for which the complexity of the experiments and the limited accuracy usually make testing of theories much more difficult. We hope the present results may encourage new soft matter experiments with more control on the initial perturbation amplitude and wavelength, similar to those reported in Ref. [53], but keeping constant the gravity acceleration g .

ACKNOWLEDGMENTS

S.A.P. warmly thanks the members of the Department of Statistical Physics and Nonlinear Dynamics of the Brandenburg University of Technology (Cottbus), for their kind and

friendly hospitality during her one-year postdoctoral stay in the Department. This work has been partially supported by the Ministerio de Economía y Competitividad of Spain (Grants

No. ENE2016-75703-R and No. BES-2017-079674), Junta de Comunidades de Castilla-La Mancha of Spain (Grant No. SBPLY/17/180501/000264), and by the BMBF of Germany.

- [1] L. Rayleigh, *Scientific Papers* (Cambridge University Press, Cambridge, 1900), Vol. II, pp. 200–207.
- [2] G. I. Taylor, *Proc. R. Soc. London Ser. A* **201**, 192 (1950).
- [3] S. Chandrasekhar, *Hydrodynamics and Hydromagnetic Stability* (Dover, New York, 1961), pp. 428–480
- [4] D. H. Sharp, *Physica D* **12**, 3 (1984).
- [5] H. J. Kull, *Phys. Rep.* **206**, 197 (1991).
- [6] S. A. Piriz, A. R. Piriz, and N. A. Tahir, *Phys. Rev. E* **97**, 043106 (2018).
- [7] Y. Zhou, *Phys. Rep.* **720–722**, 1 (2017)
- [8] W. Gorczyk, B. Gobbs, and T. Gerya, *Tectonophysics* **514–517**, 146 (2012).
- [9] O. Blaes, R. Blandford, P. D. Madau, and P. Koonin, *Astrophys. J.* **363**, 612 (1990).
- [10] S. A. Piriz, A. R. Piriz, and N. A. Tahir, *Phys. Fluids* **30**, 111703 (2018).
- [11] S. A. Piriz, A. R. Piriz, and N. A. Tahir, *J. Fluid Mech.* **867**, 1012 (2019).
- [12] S. I. Blinnikov, R. I. Ilkaev, M. A. Mochalov, A. L. Mikhailov, I. L. Iosilevskiy, A. V. Yudin, S. I. Glazyrin, A. A. Golubev, V. K. Gryaznov, and S. V. Fortova, *Phys. Rev. E* **99**, 033102 (2019).
- [13] N. A. Tahir, A. Shutov, D. Varentsov, P. Spiller, S. Udrea, D. H. H. Hoffmann, I. V. Lomonosov, J. Wieser, M. Kirk, A. R. Piriz, V. E. Fortov, and R. Bock, *Phys. Rev. ST Accel. Beams* **6**, 020101 (2003).
- [14] N. A. Tahir, A. Kozyreva, P. Spiller, D. H. H. Hoffmann, and A. Shutov, *Phys. Rev. E* **63**, 036407 (2001).
- [15] N. A. Tahir, I. V. Lomonosov, B. Borm, A. R. Piriz, A. Shutov, P. Neumayer, V. Bagnoud, and S. A. Piriz, *Astrophys. J. Suppl.* **232**, 1 (2017).
- [16] N. A. Tahir, A. Shutov, I. V. Lomonosov, A. R. Piriz, P. Neumayer, V. Bagnoud, and S. A. Piriz, *Astrophys. J. Suppl.* **238**, 27 (2018).
- [17] N. A. Tahir, P. Neumayer, A. Shutov, A. R. Piriz, I. V. Lomonosov, V. Bagnoud, S. A. Piriz, and C. Deutsch, *Contrib. Plasma Phys.* **59**, e201800143 (2019).
- [18] N. A. Tahir, A. Shutov, A. R. Piriz, P. Neumayer, I. V. Lomonosov, V. Bagnoud, and S. A. Piriz, *Contrib. Plasma Phys.* **59**, e201800135 (2019).
- [19] A. R. Piriz, J. J. López Cela, O. D. Cortazar, N. A. Tahir, and D. H. H. Hoffmann, *Phys. Rev. E* **72**, 056313 (2005).
- [20] A. R. Piriz, O. D. Cortázar, J. J. López Cela, and N. A. Tahir, *Am. J. Phys.* **74**, 1095 (2006).
- [21] J. J. López Cela, A. R. Piriz, M. C. Serna Moreno, and N. A. Tahir, *Laser Part. Beams* **24**, 427 (2006).
- [22] A. R. Piriz, J. J. López Cela, N. A. Tahir, and D. H. H. Hoffmann, *Phys. Rev. E* **78**, 056401 (2008).
- [23] B. A. Remington, P. Allen, E. M. Bringa, J. Hawreliak, D. Ho, K. T. Lorenz, H. Lorenzana, J. M. McNaney, M. A. Meyers, S. W. Pollaine, K. Rosolankova, B. Sadik, M. S. Schneider, D. Swift, J. Wark, and B. Yaakobi, *Mater. Sci. Tech.* **22**, 474 (2006).
- [24] H. S. Park, K. T. Lorenz, R. M. Cavallo, S. M. Pollaine, S. T. Prisbrey, R. E. Rudd, R. C. Becker, J. V. Bernier, and B. A. Remington, *Phys. Rev. Lett.* **104**, 135504 (2010).
- [25] A. R. Piriz, J. J. López Cela, and N. A. Tahir, *Phys. Rev. Lett.* **105**, 179601 (2010).
- [26] K. O. Mikaelian, *Phys. Plasmas* **17**, 092701 (2010).
- [27] A. R. Piriz and M. M. Sánchez, *Phys. Plasmas* **5**, 2721 (1998).
- [28] S. M. Bakhrahk, O. B. Drennov, N. P. Kovalev, A. I. Lebedev, E. E. Meshkov, A. L. Mikhailov, N. V. Neumerzhitsky, P. N. Nizovtsev, V. A. Rayevsky, G. P. Simonov, V. P. Solovyev, and I. G. Zhidov, Lawrence Livermore National Laboratory Report No. UCRL-CR-126710, 1997 (unpublished), <https://www.osti.gov/scitech/servlets/purl/515973>.
- [29] D. H. Kalantar, B. A. Remington, J. D. Colvin, K. O. Mikaelian, S. V. Weber, L. G. Wiley, J. S. Wark, A. Loveridge, A. M. Allen, A. A. Hauer, and M. A. Meyers, *Phys. Plasmas* **7**, 1999 (2000).
- [30] J. D. Colvin, M. Legrand, B. A. Remington, G. Shurtz, and S. V. Weber, *J. Appl. Phys.* **93**, 5287 (2003).
- [31] K. T. Lorenz, M. J. Eswards, S. G. Glendinning, A. F. Jankowski, J. McNaney, S. M. Pollaine, and B. A. Remington, *Phys. Plasmas* **12**, 056309 (2005).
- [32] J. K. Dienes, *Phys. Fluids* **21**, 736 (1978).
- [33] E. L. Ruden and D. E. Bell, *J. Appl. Phys.* **82**, 163 (1997).
- [34] J. F. Barnes, P. J. Blewet, R. G. McQueen, K. A. Meyer, and D. Venable, *J. Appl. Phys.* **45**, 727 (1974).
- [35] A. C. Robinson and J. W. Swegle, *J. Appl. Phys.* **66**, 2859 (1989).
- [36] A. R. Piriz, Y. B. Sun, and N. A. Tahir, *Eur. J. Phys.* **38**, 015003 (2017).
- [37] J. W. Miles, General Dynamics Report No. GAMD-7335, AD 643161 (1966) (unpublished).
- [38] G. N. White, Los Alamos National Laboratory Report No. LA-5225-MS (1973) (unpublished).
- [39] D. C. Drucker, in *Mechanics Today*, edited by S. Nemat-Nasser (Pergamon, Oxford, 1980), Vol. 5, p. 37.
- [40] D. C. Drucker, *Ing.-Arch.* **49**, 361 (1980).
- [41] S. A. Piriz, A. R. Piriz, and N. A. Tahir, *Phys. Rev. E* **95**, 053108 (2017).
- [42] A. R. Piriz, J. J. López Cela, and N. A. Tahir, *Phys. Rev. E* **80**, 046305 (2009).
- [43] A. R. Piriz, J. J. López Cela, and N. A. Tahir, *J. Appl. Phys.* **105**, 116101 (2009).
- [44] A. R. Piriz, Y. B. Sun, and N. A. Tahir, *Phys. Rev. E* **89**, 063022 (2014).
- [45] Y. B. Sun and A. R. Piriz, *Phys. Plasmas* **21**, 072708 (2014).
- [46] B. J. Plohr and D. H. Sharp, *Z. Angew. Math. Phys.* **49**, 786 (1998).
- [47] S. A. Piriz, A. R. Piriz, and N. A. Tahir, *Phys. Rev. E* **96**, 063115 (2017).
- [48] G. Terrones, *Phys. Rev. E* **71**, 036306 (2005).

- [49] S. Mora, T. Phou, J.-M. Fromental, and Y. Pomeau, *Phys. Rev. Lett.* **113**, 178301 (2014).
- [50] D. Riccobelli and P. Ciarletta, *Philos. Trans. R. Soc. A* **375**, 20160421 (2017).
- [51] A. Chakrabarti, S. Mora, F. Richard, T. Phou, J.-M. Fromental, Y. Pomeau, and B. Audoly, *J. Mech. Phys. Solids* **121**, 234 (2018).
- [52] I. Maimouni, J. Goyon, E. Lac, T. Pringuey, J. Boujlel, X. Chateau, and P. Coussot, *Phys. Rev. Lett.* **116**, 154502 (2016).
- [53] R. Polavarapu, P. Roach, and A. Banerjee, *Phys. Rev. E* **99**, 053104 (2019).
- [54] A. R. Piriz, S. A. Piriz, and N. A. Tahir, *Phys. Rev. E* **100**, 063104 (2019).
- [55] W. F. Chen, *Limit Analysis and Soil Plasticity* (Elsevier, Amsterdam, 1975).
- [56] R. Menikoff, R. C. Mjølness, D. H. Sharp, C. Zemach, and B. J. Doyle, *Phys. Fluids* **21**, 1674 (1978).
- [57] A. C. Eringen and E. S. Suhubi, *Elastodynamics. Vol. II: Linear Theory* (Academic, New York, 1975).
- [58] K. S. Thorne and R. G. Blandford, *Modern Classical Physics* (Princeton University Press, Oxford, 2017), Chap. 12.
- [59] M. E. Gurtin and L. Anand, *J. Mech. Phys. Solids* **53**, 1624 (2005).
- [60] K. O. Mikaelian, *Phys. Rev. A* **42**, 7211 (1990).